

Modeling of octagonal concrete-filled double-skin steel tube stub columns under axial compression

Shagea Alqawzai^{1*}, Bo Yang², Belal Alsubari³, Hayder Saadon Abdulaali⁴ and Mohamed Elchalakani⁵

¹Ph.D Candidate, School of Civil Engineering, Chongqing University, Chongqing 400045, China

²Professor, School of Civil Engineering, Chongqing University, Chongqing 400045, China

³Assistance Professor, Department of Civil Engineering, Faculty of Engineering, Miami College of Henan University, Kaifeng, Henan, China

⁴Ph.D Candidate, Department of Architecture, Faculty of Engineering and Built Environment, University of Kebangsaan Malaysia, Bangi, Selangor, Malaysia

⁵Professor, School of Civil, Environmental and Mining Engineering, The University of Western Australia, Crewley, WA 6009, Australia

*Corresponding author: engshagea2017@gmail.com

ABSTRACT

Received: 26 January 2022

Accepted: 15 March 2022

Octagonal concrete-filled double-skin steel tube (OCFDST) columns have drawn the attention of academia and building industries since they combined the advances of higher confinement of circular CFDST columns and the better constructability options of square CFDST columns. Therefore, this paper investigates numerically the behavior of axially compressed OCFDST stub columns by the means of finite element analysis employing ABAQUS software. The accuracy of the developed finite element (FE) models was validated against the experimental results in terms of axial load-axial shortening curves and the ultimate strength of the test specimens. Then, subsequent parametric studies considering a wide range of outer parameters were performed by the verified FE model on the effects of various parameters including the thickness of outer steel tube (t_o), the thickness of inner steel tube (t_i), the diameter of inner steel tube (D_i) and type and arrangement of stiffening schemes. The numerically generated data were then used to evaluate the applicability of the design guidelines provided by existing European, North American, and Chinese provisions for composite columns. Based on the results, it was found that EC4 and modified EC4 formulas can safely be adopted to predict the design ultimate strength of OCFDST stub columns. AISC360 can also give a reasonable for non-stiffened specimens while, DBJ provides un-conservative predictions of ultimate strength when applied to non-stiffened OCFDST stub columns, while it can accurately calculate the ultimate strength of the OCFDST axial members with different stiffening schemes.

Keywords: octagonal concrete-filled double-skin tube; stub column; finite element modeling; stiffening schemes; ultimate capacity; ductility

Introduction

The adoption of concrete-filled steel tubes (CFSTs) in modern construction has been increasingly growing due to their excellent performance. Innovative composite members were derived from the conventional CFST members, known as concrete-filled double steel tubes (CFDSTs). CFDSTs are composite members, which consist of two



concentric steel layers and sandwiched concrete in between them. They have the same characteristics as CFSTs and have less weight. The applications of CFDST columns were found to provide better structural performance over their conventional CFST counterparts in terms of load capacity, ductility, stiffness, global and local stability, and fire performance owing to the excellent interaction between their components and increased section modulus [1-3]. CFDST axial members with circular sections provide an ideal confinement effect because the confining stress in the concrete is uniform and isotropic across the section. In comparison, for the counterpart with the rectangular section, the confining stress in the concrete is non-uniform and anisotropic, which generally leads to a low increase in axial capacity. However, the former ones are mostly preferred in designing composite columns attributing to their ease of connection to the steel beams. Besides, in some studies [4-7], stiffening methods/schemes have been used for enhancing the confining pressure of rectangular sections, as shown in Figure 1. Moreover, CFDST members with octagonal sections can suit the architectural and functional requirements of CFDST members because they provide greater confinement than that induced by the rectangular sections and ease of connection to the steel beam compared to circular sections. Extensive research has been performed to investigate the performance of circular [8-12] and square [13, 14] CFDST columns. Besides, considerable research works have been done to evaluate the behavior of OCFST columns [15-17]. However, the studies on OCFDST stub columns are still very scarce. Yang et al. [18] experimentally and numerically evaluated the performance of concrete-filled double skin steel tube (CFDSST) members with the octagonal outer tube and circular inner layer under axial compression. Yuan and Yang [19] also presented experimental and numerical investigations on the performance of concrete-filled double skin composite tube columns (CFDSCT) composed of an octagonal steel tube as its outer steel layer, a circular PVC pipe as its inner layer, and high strength concrete-filled in between them.

Owing to the limited research studies, international codes of practice such as Eurocode 4 [20], AISC 360-16 [21], and DBJ/T13-51-2010 [22] have not included design rules for such composite columns. This paper aims to carry out finite element (FE) modeling using ABAQUS software to simulate the behavior of OCFDST stub columns under axial load. The FE-generated results were therefore verified by the experimental results obtained in [6].

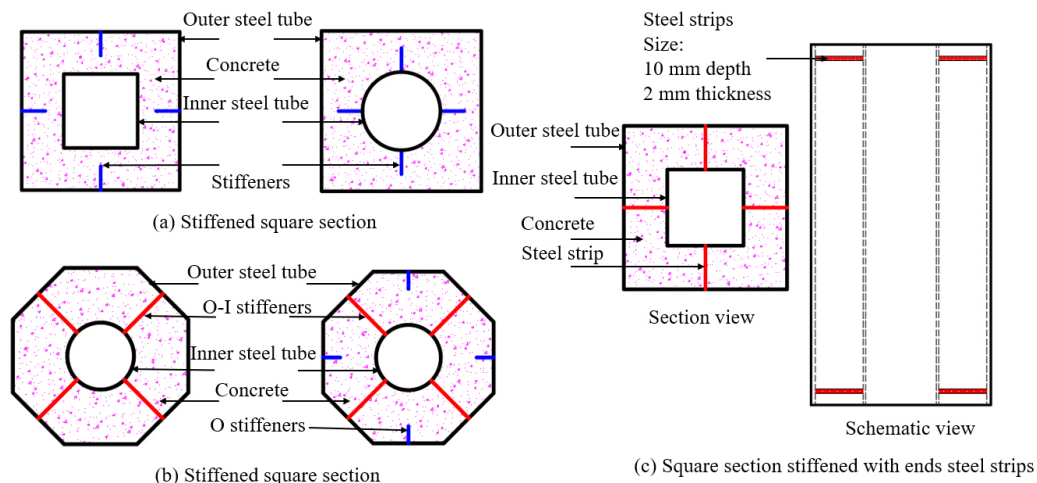


Figure 1. Previously adopted stiffening schemes.

Moreover, the FE predicted ultimate loads were compared with the estimated ultimate strength from the current international design codes of practice.

Finite Element Modelling

General Description

A series of three-dimensional finite element models using the ABAQUS software package has been developed. Eight-nodded solid element (C3D8R) and four-nodded shell element (SR4) with decreased integration were adopted to simulate the sandwiched concrete and the steel metals of the studied specimens, respectively. A mesh convergence study was conducted to determine the appropriate mesh type, numbers, or/and size to attain reliable simulations with a reasonable numerical model and less computational time. Considering the prediction accuracy and computational time, the convergence study indicates that a number of 25 mesh can be used in the longitudinal direction, while a number of 5 and 48 mesh can be maintained for the radial and circumferential directions of the cross-section, respectively. A sweep meshing option was utilized with a typical mesh shown in Figure 2.

Material Models

Confined Concrete Model

The three-stage stress-strain model depicted in Figure 3 is used to represent the behavior of the sandwiched concrete in OCFDST short columns under axial compression [23]. The ascending first part (OA) of the stress-strain curve is represented by the equation suggested by [24] for confined sandwiched concrete as expressed by Eq. (1):

$$\sigma_c = \frac{f'_{cc}(\epsilon_c/\epsilon'_{cc})^\lambda}{(\epsilon_c/\epsilon'_{cc})^\lambda + \lambda - 1} \text{ for } 0 \leq \epsilon_c \leq \epsilon'_{cc} \quad (1)$$

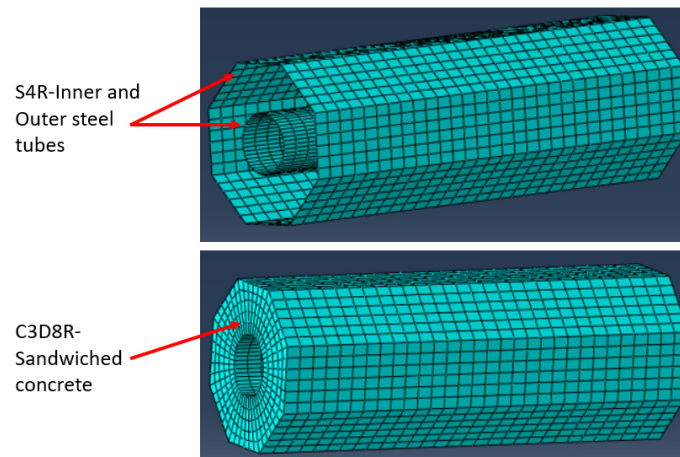


Figure 2. Typical mesh adopted for simulating OCFDST stub columns.

where, σ_c and ϵ_c represent the axial stress, and the corresponding compressive strain, respectively. f'_{cc} and ϵ'_{cc} denote the compressive strength of confined concrete and its corresponding confined strain, respectively. λ is a factor that controls the curvature and initial slope of the ascending part and calculated by Eq. (2):

$$\lambda = \frac{\epsilon'_{cc} E_c}{\epsilon'_{cc} E_c - f'_{cc}} \quad (2)$$

where, E_c is the concrete elastic modulus of elasticity proposed by [25] and modified by [26] to take into account the influence of column size, as given in Eq. (3):

$$E_c = 4400 \sqrt{\gamma_c f'_c} \text{ (MPa)} \quad (3)$$

in which, γ_c is the reduction factor taking into account the influence of the column size, proposed by [27] as given by Eq. (4):

$$\gamma_c = 1.85 D_c^{-0.135} \quad (0.85 \leq \gamma_c \leq 1) \quad (4)$$

where, D_c designates the diameter of concrete in the CFDST stub column with octagonal or circular sections, taken as $(D_o - 2t_o)$, where D_o represents the diameter of the outer steel tube, while t_o denotes its thickness. The maximum confined strength (f'_{cc}) and its corresponding strain (ϵ'_{cc}) of the concrete are calculated by the equations provided by [24] taking into account the factor given by [28] as provided in Eq. (5) and Eq.(6), respectively:

$$f'_{cc} = \left(1 + \frac{K_1 f_{rpo}}{\gamma_c f'_c} \right) (\gamma_c f'_c) \quad (5)$$

$$\epsilon'_{cc} = \left(1 + \frac{K_2 f_{rpo}}{\gamma_c f'_c} \right) \epsilon'_c \quad (6)$$

in which, (f_{rpo}) represents the confining pressure on the sandwiched concrete, K_1 and K_2 are constants provided by [29], taken as 4.1 and 20.5, respectively, and ϵ'_c is the strain corresponds to the unconfined concrete compressive strength (f'_c) determined by an equation derived by [28] as written in Eq. (7):

$$\epsilon'_c = \begin{cases} 0.002 & \text{for } \gamma_c f'_c \leq 28 \text{ (MPa)} \\ 0.002 + \frac{(\gamma_c f'_c - 28)}{54000} & \text{for } 28 < \gamma_c f'_c \leq 82 \text{ (MPa)} \\ 0.003 & \text{for } \gamma_c f'_c > 82 \text{ (MPa)} \end{cases} \quad (7)$$

In this paper, the lateral confining pressure on the sandwiched concrete (f_{rpo}) in CFDST columns constructed of the octagonal section is determined by the equation provided by [30], as expressed in Eq. (8):

$$\frac{f_{rpo}}{f_{yo}} = \begin{cases} 0.043646 - 0.000832 \left(\frac{D_o}{t_o} \right) & \text{for } 21.7 \leq \frac{D_o}{t_o} \leq 47 \\ 0.006241 - 0.0000357 \left(\frac{D_o}{t_o} \right) & \text{for } 47 < \frac{D_o}{t_o} \leq 150 \end{cases} \quad (8)$$

Two linear descending parts (AB) and (BC) of the stress-strain curve for confined concrete can be determined by the expression in Eq. (9):

$$\sigma_c = \begin{cases} f'_{cc} + (f_e - f'_{cc}) \left(\frac{\epsilon_c - \epsilon'_{cc}}{\epsilon_e - \epsilon'_{cc}} \right) & \text{for } \epsilon'_{cc} < \epsilon_c \leq \epsilon_e \\ f_e + (f_{cu} - f_e) \left(\frac{\epsilon_c - \epsilon_e}{\epsilon_{cu} - \epsilon_e} \right) & \text{for } \epsilon_e < \epsilon_c \leq \epsilon_{cu} \end{cases} \quad (9)$$

Where ϵ_e and ϵ_{cu} are compressive strains of concrete at points B and C as shown in Figure 3. The compressive strain ϵ_e is taken as, $10\epsilon'_c$ corresponding to point B. The compressive strain ϵ_{cu} at point C is taken as, $30\epsilon'_c$. f_e and f_{cu} are the stresses corresponding to strains ϵ_e and ϵ_{cu} , respectively, given in Eq. (10) and Eq. (11), respectively:

$$f_e = \alpha_c f'_{cc} \quad (10)$$

$$f_{cu} = \beta_c f'_{cc} \quad (11)$$

where α_c and β_c denote the effect of confinement on the ductility of concrete in the post-peak branch, given by the equation suggested by [31], as denoted by Eq. (12) and Eq. (13), respectively:

$$\alpha_c = 0.9729 - 0.0091 \gamma_c f'_c \quad (12)$$

$$\beta_c = 0.9987 - 0.0107 \gamma_c f'_c \quad (13)$$

The Drucker-Prager criterion for simulating the confined concrete in circular, elliptical, and OCFST columns [32] is adopted. The constant values of 20° , 0.8 and 30° are assumed for friction angle, flow-stress ratio, and dilation angle in defining the Drucker-Prager parameters based on sensitivity study.

Material Model for Steel Tubes

The steel tube of the axially-compressed OCFDST stub column is under bi-axial stresses attributing to the influence of steel tube confinement on the sandwich concrete. This phenomenon reduces the longitudinal yield stress of the steel tube [25, 27]. The yield stress of steel is multiplied by a factor of 0.9 to consider this effect. The equation proposed by [25] is used to predict the rounded part of the curve as shown in Eq. (14):

$$\sigma_s = f_{sy} \left(\frac{\epsilon_s - 0.9\epsilon_{sy}}{\epsilon_{st} - 0.9\epsilon_{sy}} \right)^{\frac{1}{45}} \quad (14)$$

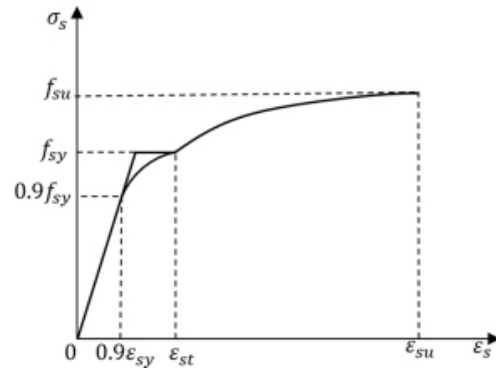
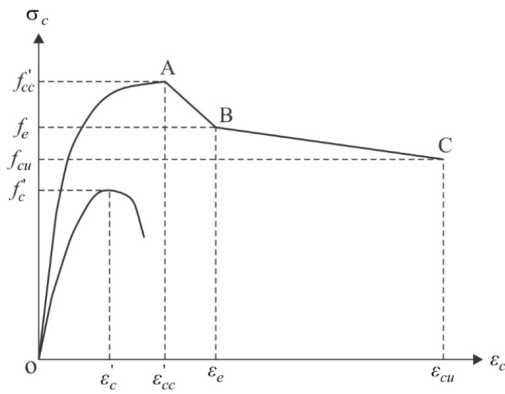


Figure 3. A general stress-strain curve of concrete confined [23]. **Figure 4.** General stress-strain curve for structural steels [24].

where σ_s describes the axial steel stress, ϵ_s denotes the axial steel strain, ϵ_{sy} is the yield strain corresponding to the yield strength (f_{sy}), and ϵ_{st} is the strain at the onset of strain hardening, taken as 0.005 in this study. The stresses after the strain hardening are calculated by utilizing the equations proposed by [24], expressed in Eq. (15):

$$\sigma_s = f_{su} - \left(\frac{\epsilon_{su} - \epsilon_s}{\epsilon_{su} - \epsilon_{st}} \right)^n (f_{su} - f_{sy}) \tag{15}$$

$$n = E_{st} \left(\frac{\epsilon_{su} - \epsilon_{st}}{f_{su} - f_{sy}} \right) \tag{16}$$

in which, f_{su} represents the steel tensile strength, $\epsilon_{su} = 0.2$ is the ultimate strain and E_{st} designates the steel modulus of elasticity at the onset of strain-hardening and a value of $E_{st} = 0.02 E_s$ is used. The General stress-strain curve for steel is illustrated in Figure 4.

Interaction, Boundary Conditions, and Loading

Surface-to-surface interaction is utilized to model the interaction between the metal and concrete in this study [1, 5, 17]. Hard contact condition was specified to simulate the behavior in the normal direction designated by avoiding the surface penetration in compression and allowing the separation in tension [33, 34], while the Coulomb friction model with penalty friction and directionality of isotropic was adopted to simulate the interface in the tangential direction. For CFDST short columns, as the steel tubes and concrete deformed together under axial compression, it was assumed that there is little or no slip between the steel tubes and sandwiched concrete. For this reason, it was found that the behavior of CFDST stub columns is not sensitive to the friction coefficient selection between the steel and concrete [34]. Therefore, frictional coefficients of 0.25 were adopted in this study. For the longitudinal stiffeners, these components were merged with the steel tubes in a single part, hence the interaction between the steel tubes and stiffeners was considered by the inherent way of sharing common nodes. Although the longitudinal stiffeners were merged with the steel tubes, they were embedded into the sandwiched concrete [5, 33]. Since the

end-stiffeners or/and clamps were not included [6], the steel and concrete are in normal contact with the stiff platens of the testing machine directly [5]. To replicate the end-friction provided by the testing machine, all three translation degrees of freedom can be restrained at all ends of the column except the displacement at the loaded end in the direction of loading. Meanwhile, the rotational degrees of freedom for both ends of the columns are not restrained which is known as pinned end-conditions. A uniformly distributed load was directly applied at the top of the specimens using a displacement control approach with a maximum displacement of 0.01 mm.

Verification of FE Modeling

The results of both developed finite element (FE) models were verified and compared against the experimental data reported in [6]. In the experimental investigation conducted by [6], a total of eight OCFDST stub columns were experimentally tested under axial compression, which is used to ensure the accuracy of the FE models. The actual slenderness ratio (w/t_o) that is described as the ratio of the measured side of the width of the outer octagonal steel tube (w_o) to its thickness (t_o) was 45.52 for all the test specimens. The measured slenderness ratio was kept greater than that calculated by the slenderness limit specified in ASCE 48-11 [35]. ASCE 48-11 [35] specified the limit for slenderness ratio $(w/t_o)_{Limit} \leq 681.2/\sqrt{f_{yo}}$, where f_{yo} is the actual yield of the stress of the outer steel tube. The details of cross-sections for the experimental specimens are summarized in Table 1. The overall comparison between FE-predicted results and test data is conducted by considering load-axial deformation ($N-\Delta$) curves and ultimate design strengths. It can be observed from Figure 5 that the FE-simulated ($N-\Delta$) curves are in good agreement with their experimental counterparts. Additionally, the numerically predicted ultimate strengths ($N_{u, FEM}$) are similar with those obtained from experimental tests, ($N_{u, Test}$) as can be seen from Table 2. Table 2 provides details on material properties and overall comparison between FE-predicted and experimental ultimate strengths through considering the ratio ($N_{u, FEM}/N_{u, Test}$). It is found that the mean ratio of ($N_{u, FEM}/N_{u, Test}$) is 0.97 with a corresponding standard deviation (SD) of 0.004 indicating that the adopted concrete model is capable to replicate accurately the test results of OCFDST stub columns under axial compression. Accordingly, an extensive parametric study is performed over a wide range of parameters as shown in the following sections.

Table 1. Cross-sectional details for the experimental OCFDST stub columns

Column Label	L (mm)	Outer steel Tube				Inner Steel Tube		O-I stiffener		O Stiffener		(w/t_o)	(w/t_o) limit
		D_o (mm)	H (mm)	w (mm)	t_o (mm)	D_i (mm)	t_i (mm)	b_{soi} (mm)	t_{soi} (mm)	b_{so} (mm)	t_{so} (mm)		
O1S00	900.0	300.0	324.72	124.27	2.73	114.0	4.00	0.0	0.0	0.0	0.0	45.52	31.10
OP1S00	900.0	300.0	324.72	124.27	2.73	114.0	4.00	93.0	2.73	0.0	0.0	45.52	31.10
OP1S30	900.0	300.0	324.72	124.27	2.73	114.0	4.00	93.0	2.73	30	2.73	45.52	31.10
OP1S57	900.0	300.0	324.72	124.27	2.73	114.0	4.00	93.0	2.73	57	2.73	45.52	31.10

where, b_{soi} and b_{so} are the embedded width of O-I, and O longitudinal stiffeners, respectively, while t_{soi} and t_{so} denote the thickness of the same.

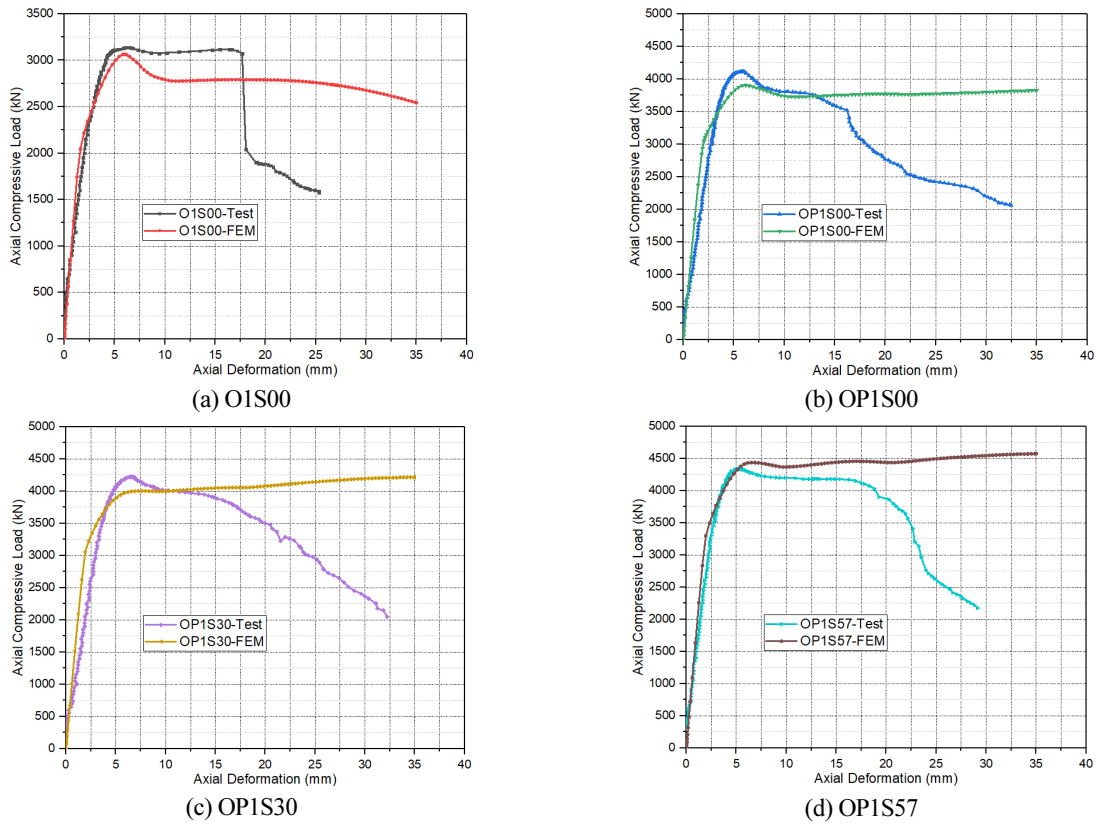


Figure 5. Comparison of ($N-\Delta$) curves between test results and FE predictions.

Table 2. Material properties and overall comparison of stub columns test with FE-generated results

Column Label	f_{yo} (MPa)	f_{yi} (MPa)	f_{uo} (MPa)	f_{ui} (MPa)	E_{so} (GPa)	E_{si} (GPa)	f_{cu} (MPa)	$N_{u,exp}$ (kN)	$N_{u,FEM}$ (kN)	$N_{u,FEM}/N_{u,exp}$
O1S00	468.3	437.3	590.1	615.8	212.6	191.7	42.5	3139	3066.67	0.98
OP1S00	468.3	437.3	590.1	615.8	212.6	191.7	42.5	4117.7	3904.69	0.95
OP1S30	468.3	437.3	590.1	615.8	212.6	191.7	38.4	4222.4	4002.57	0.95
OP1S57	468.3	437.3	590.1	615.8	212.6	191.7	42.5	4340	4437.00	1.02
								Mean		0.97
								Standard Deviation (SD)		0.004

Parametric Study

General Description

To fully understand the behavior of OCFDST columns under axial compression, there is a need to conduct further parametric analysis to cover a wider range of parameters. Possible parameters influencing the performance of these stub columns include the outer steel tube thickness (t_o), inner steel tube thickness (t_i) and its diameter (D_i) as well as the arrangements and schemes of stiffening methods. In this study, three types of stiffening methods are selected for evaluating the effects of stiffeners arrangements and schemes on the behavior of OCFDST short

columns under axial compression. The outer and inner steel tubes are welded together by a steel plate, termed as outer-inner steel tubes plate stiffeners (O-I plate stiffeners). The O stiffeners are only welded to the outer tube, while T-shaped stiffeners are welded to the outer tube are also welded to either inner or outer steel tube. Cross-sectional dimensions of the stiffeners are summarized in Table 3 with a schematic illustration of stiffening schemes shown in Figure 6.

The effects of the studied parameters are assessed in terms of load-axial deformation ($N-\Delta$) curves, ultimate strength (N_u), ultimate resistance enhancement index (RI), and ductility enhancement index (DI). The RI is known as the ratio of ultimate load of the specimens to that of the reference specimens, defined by, $RI = N_{us}/N_{ur}$, in which N_{us} represents the ultimate load of selected specimens and N_{ur} denotes the ultimate load of the reference specimens, while DI is defined as the ratio of is the ductility of the selected specimens and (μ_r) to the ductility of the reference specimen [6], expressed as $DI = \mu_s/\mu_r$. The ductility of OCFDST stub columns is described as the axial-deformation at the peak load (Δ_u) to the axial-deformation when the load falls to 85% of the ultimate load ($\Delta_{95\%}$) [3], represented by, $\mu = \Delta_{95\%}/\Delta_u$.

Table 3. Cross-sectional dimensions of stiffeners

Specimen	O-I stiffener		O stiffener		T-shape Stiffener		
	b_{ois} (mm)	t_{ois} (mm)	b_{os} (mm)	t_{os} (mm)	h_{Ts} (mm)	b_{Ts} (mm)	t_{Ts} (mm)
P1S00	90.27	2.73	0	0	-	-	-
P1S30	90.27	2.73	30	2.2	-	-	-
P2S57	90.27	2.20	57	2	-	-	-
P3TO4	90.27	2	-	-	35	30	2
P3TI4	90.27	2	-	-	35	30	2
TO8	-	-	-	-	40	30	2.2

Where, h_{Ts} , b_{Ts} , and t_{Ts} denote the height, breadth, and thickness of T-shaped stiffeners

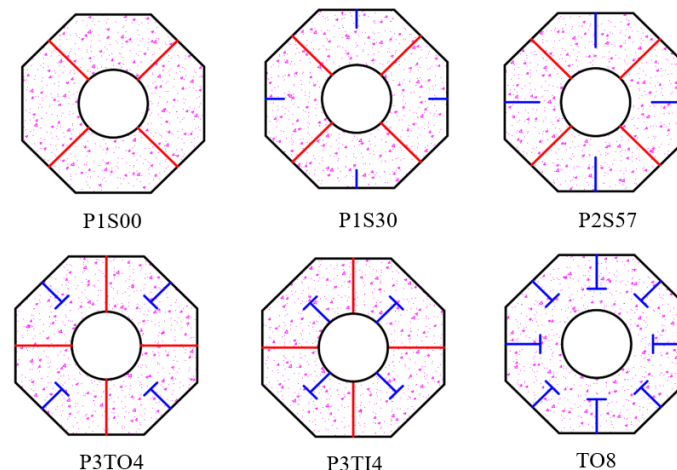


Figure 6. Schematic representations of stiffening schemes on OCFDST stub columns.

Table 4. Cross-sectional details and FE-predicted results of specimens used for parametric analysis

Specimen ID	D_o (mm)	w (mm)	t_o (mm)	D_i (mm)	t_i (mm)	w_o/t_o Ratio	D_i/t_i Ratio	f'_c (MPa)	f_{yo} (MPa)	f_{yi} (MPa)	E_o (GPa)	E_i (GPa)	N_u FEM (kN)
OS00-to2	300	124.27	2	114	4	62.14	28.50	28.8	468.3	437.3	212.1	191.7	2845.28
OS00-to3	300	124.27	3	114	4	41.42	28.50	28.8	468.3	437.3	212.1	191.7	3155.35
OS00-to4	300	124.27	4	114	4	31.07	28.50	28.8	468.3	437.3	212.1	191.7	3513.88
OS00-to5	300	124.27	5	114	4	24.85	28.50	28.8	468.3	437.3	212.1	191.7	3901.24
OS00-ti2	300	124.27	2.73	114	2	45.52	57.00	28.8	468.3	437.3	212.1	191.7	2744.19
OS00-ti3	300	124.27	2.73	114	3	45.52	38.00	28.8	468.3	437.3	212.1	191.7	2903.67
OS00-ti4	300	124.27	2.73	114	4	45.52	28.50	28.8	468.3	437.3	212.1	191.7	3066.67
OS00-ti5	300	124.27	2.73	114	5	45.52	22.80	28.8	468.3	437.3	212.1	191.7	3225.46
OS00	300	124.27	2.73	-	-	45.52	-	28.8	468.3	437.3	212.1	191.7	2691.66
OS00-Di100	300	124.27	2.73	100	4	45.52	20.00	28.8	468.3	437.3	212.1	191.7	3024.88
OS00-Di100	300	124.27	2.73	100	4	45.52	25.00	28.8	468.3	437.3	212.1	191.7	3051.15
OS00-Di120	300	124.27	2.73	120	4	45.52	30.00	28.8	468.3	437.3	212.1	191.7	3068.56
OS00-Di140	300	124.27	2.73	140	4	45.52	35.00	28.8	468.3	437.3	212.1	191.7	3058.28
OS00-Di160	300	124.27	2.73	160	4	45.52	40.00	28.8	468.3	437.3	212.1	191.7	3033.15
OS00-Di180	300	124.27	2.73	180	4	45.52	45.00	28.8	468.3	437.3	212.1	191.7	2985.6
OS00-Di200	300	124.27	2.73	200	4	45.52	50.00	28.8	468.3	437.3	212.1	191.7	2907.42
OP1S00	300	124.27	3	114	4	41.42	28.50	28.8	468.3	437.3	212.1	191.7	4026.18
OP1S30	300	124.27	2.73	114	4	45.52	28.50	28.8	468.3	437.3	212.1	191.7	4258.65
OP2S57	300	124.27	2.73	114	4	45.52	28.50	28.8	468.3	437.3	212.1	191.7	4259.11
OP3TO4	300	124.27	2.73	114	4	45.52	28.50	28.8	468.3	437.3	212.1	191.7	4296.76
OP3TI4	300	124.27	2.73	114	4	45.52	28.50	28.8	468.3	437.3	212.1	191.7	4200.4
OTO8	300	124.27	2.73	114	4	45.52	28.50	28.8	468.3	437.3	212.1	191.7	4132.18

Cross-sectional details and the selected specimens' material properties for the parametric analysis are given in Table 4. New naming terms are given for parametric due to the variation in the cross-sectional properties. The OCFDST specimens were labeled to identify easily the outer and inner steel tubes thickness, the diameter of circular inner tubes, and type of stiffening schemes and their arrangement. For instance, the first letter "O" for all specimens designates the octagonal cross-section, while numbers 2, 3, 4, and 5 following symbols t_o and t_i represented the thickness of outer and inner tubes in mm . The symbol D_i denotes the diameter of the inner tube (D_i) followed by its value in mm . "P", "T", and "S" letters refer to the O-I stiffeners, O stiffeners, and T-shaped stiffeners, respectively, while the embedded width of stiffeners are signified by numbers 1 and 2 for O stiffeners of 30 mm (width) x 2.2 mm (thickness) and 57 mm (width) x 2 mm (thickness). The numbers 4 and 8 mean that T stiffeners are welded in four and eight sides of steel tube or four segments of inner steel tube.

Effect of Outer Tube Thickness (t_o)

The thickness of the outer steel tube is a key parameter in controlling the performance of CFDST axial members

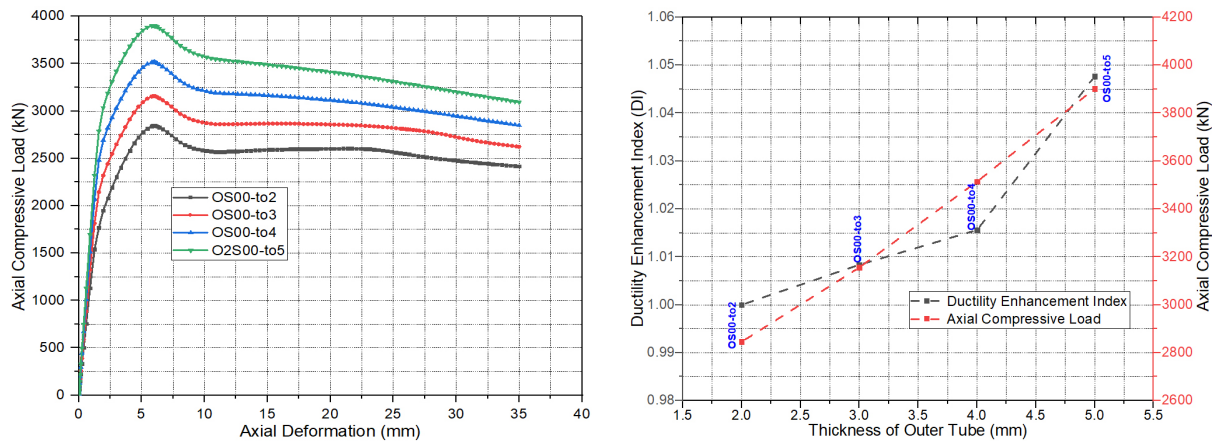


Figure 7. Effects of (t_o) on axial load-deformation curves of **Figure 8.** Effects of (t_o) on strength and ductility of OCFDST stub columns.

because it affects the confinement and mode of buckling of such specimens. Figure 7 illustrates the axial load versus axial deformation ($N-\Delta$) curves. It can be observed that the thickness of the outer steel tube (t_o) has no obvious effect on the initial part of the ($N-\Delta$) curves. However, thickness (t_o) significantly influences the ultimate strength (N_u) of OCFDST stub columns. When the thickness (t_o) increases, the ultimate strength (N_u) greatly increases. As shown in Figure 8 that the N_u increases with increasing the thickness (t_o) from 2 mm to 5 mm showing higher resistance enhancement index RI. It can be seen that, as compared to specimen OS00-to2, the ultimate strengths of specimens OS00-to3, OS00-to4, and OS00-to5 achieved an increment in the ultimate strength of 11, 23, and 37% as shown in Figure 8. This means that the specimens with larger outer tube thickness (t_o) can resist greater loads owing to the higher confinement effect of outer steel on the sandwich concrete in OCFDST stub columns. Similarly, specimens of larger thickness (t_o) higher ductility enhancement indices (DIs) owing to the contribution of steel ratio (δ_s) of the enlarged thickness of outer tube (t_o), which provides higher confinement on the sandwiched concrete leading to higher ductility of the OCFDST stub columns. Overall, it can be concluded that using thicker out steel tubes can impose a higher confinement effect on the sandwiched concrete resulting in higher ultimate strength (N_u) and ductility.

Effect of Inner Tube Thickness (t_i)

Figure 9 elucidates the effect of different thicknesses of inner steel tubes on the axial load versus axial deformation ($N-\Delta$) curves. It can be seen that using a bigger thickness of the inner tube (t_i) does not the initial stiffness (elastic branch) of the ($N-\Delta$) curves. However, increasing the thickness (D_o) can impose a considerable on the ultimate strength (N_u) of the OCFDST specimens. It can be observed that the specimen OS00-ti5 with thickness (t_i) *affect* of 5 mm attained the highest ultimate strength (N_u) of 3225.46 kN with resistance enhancement index (RI) of 1.18, as compared with the reference specimen OS00-ti2 with the smaller thickness (t_i) of 2 mm, which achieved the lowest N_u value of 2744.19 kN (RI=1). Specimens OS00-ti3 ($t_i = 3\text{ mm}$), OS00-ti4

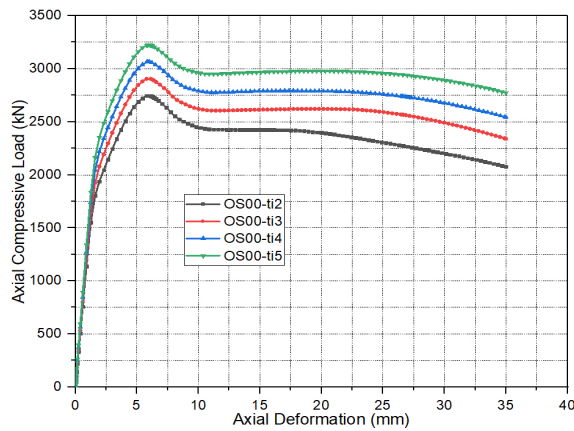


Figure 9. Effects of (t_i) on axial load-deformation curves of OCFDST stub columns.

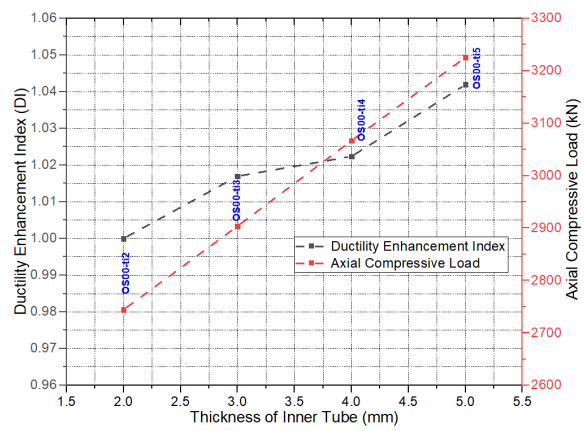


Figure 10. Effects of (t_i) on strength and ductility of OCFDST stub columns.

($t_i = 4\text{ mm}$) also attained a higher ultimate load (N_u) of 2903.67 and 3066.67 kN with RI values of 1.06 and 1.12, respectively. This indicates that increasing the thickness (t_i) can impose an increase of 6% in the ultimate strength (N_u) of OCFDST stub columns. As it can be observed from Figure 10 that increasing the thickness (t_i) can slightly enhance the ductility of the specimens with higher DI of 1.04% achieved for specimen OS00-ti5. Overall, it can be concluded that increasing the thickness of the inner steel tube can result in a considerable enhancement on the ultimate strength (N_u) of OCFDST stub columns with a minor ductility improvement. This could be because using thicker inner tubes does not contribute to the confinement of sandwiched concrete and only affects the strength of OCFDST stub columns rather than their ductility.

Effect of Inner Tube Diameter (D_i)

The thickness of inner steel tubes (D_i) is an essential parameter for evaluating the performance of OCFDST stub columns taking into consideration the reduction in material and weight of the axial structural members. It can be observed from Figure 11 that using the larger diameter of the inner steel tube increases the ultimate strength of OCFDST stub specimens. It can be observed from Figure 12 that as compared with other specimens, the specimens (OS00-Di120 and OS00-Di140) attain the highest ultimate load (N_u) of 3068.56 and 3058.28 kN , while the reference specimen (OS00) achieved the lowest ultimate strength (N_u) of 2691.66 kN . Besides, it can be noticed that the strengths of OCFDST stub columns significantly increase with increasing the diameter of the inner tube (D_i) up to 140 mm. However, further increases in D_i can adversely affect the strength of OCFDST short axial members. As compared to reference specimen (OS00), it can be found that specimens with D_i of 80, 100, 120, 140, 160, 180, and 200 mm achieved RIs values of 1.12, 1.13, 1.14, 1.14, 1.13, 1.11, and 1.08, respectively. In addition, the reference specimen showed the best ductility performance, as compared to other specimens. It can be found from Figure 12 that the DI results are scattered along with using different diameters (D_i). This could be due to the scattered effects of the hollow ratio (ψ_o) and steel ratio (δ_s) in affecting the ductility of OCFDST stub specimens.

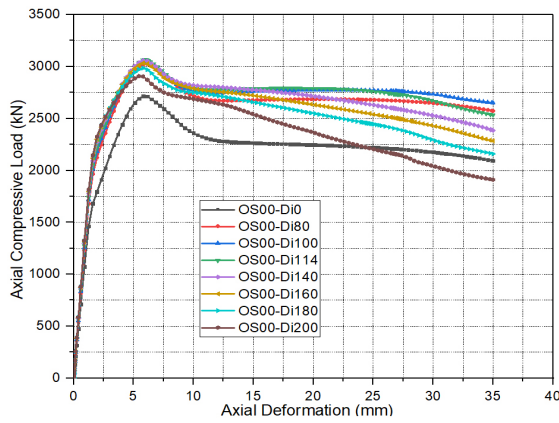


Figure 11. Effects of (D_i) on axial load-deformation curves of OCFDST stub columns.

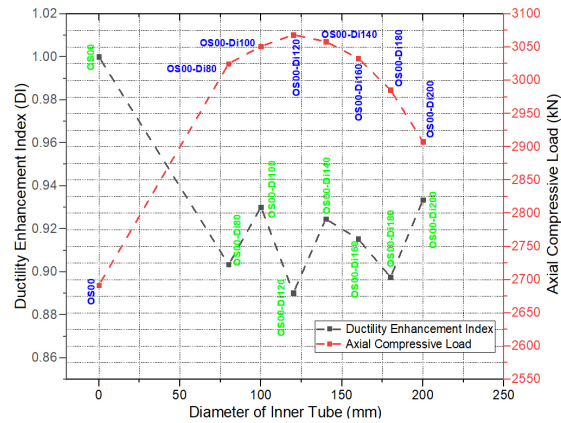


Figure 12. Effects of (D_i) on strength and ductility of OCFDST stub columns.

Overall, in order to achieve the best utilization of materials in terms of performance enhancement and weight reduction, OCFDST axial members should be designed using an appropriate diameter (D_i).

Effect of Stiffening Schemes

The stiffeners are used herein to compare the effects of different stiffening schemes on the mechanical behavior of stiffened OCFDST stub columns by evaluating their contribution in preventing the elastic-plastic buckling of specimens. For this proposal, the steel ratio (δ_s) was nearly kept the same in the range of (7.52-7.56%) for all stiffened specimens, except for specimen (OP2S57, $\delta_s = 8.11\%$). The steel ratio (δ_s) for the unstiffened specimen (OS00-to4) was kept at 7.66%. It can be seen from Figure 13 that the stiffening methods have a remarkable effect on the softening branch of ($N-\Delta$) curves. The softening branch shows a ductile response for all the stiffened specimens as compared with their unstiffened counterpart. Therefore, this demonstrates that strengthening OCFDST stub columns by welding steel plate stiffeners can significantly enhance the strength and ductility of these

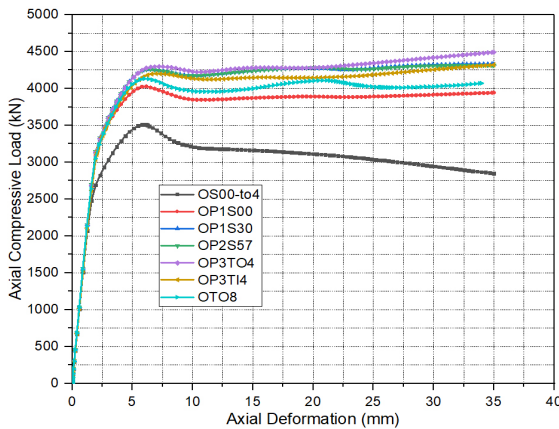


Figure 13. Effects of stiffening methods on load-displacement curves of OCFDST stub columns.

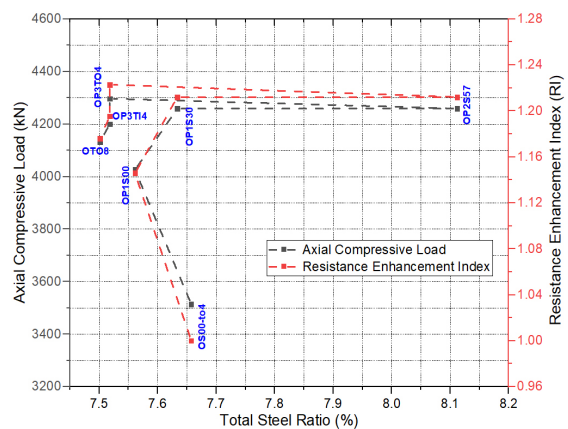


Figure 14. Effects of stiffening methods on strength and ductility of OCFDST stub columns.

types of axial members. Additionally, as compared with the reference specimen (OS00-to4), it can be seen from Figure 14 that the specimen (OP3TO4, $\delta_s = 7.52\%$), strengthening by welding four T-shaped stiffeners to the outer tube attained the highest ultimate strength (N_u) of 4296.76 kN with resistance enhancement index (RI) of 1.22, followed by specimens OP2S57, OP1S30, OP3TI4, OTO8, and OP1S00 with ultimate strengths (N_u) of 4259.11, 4258.65, 4200.4, 4132.18, and 4026.18 kN with corresponding RI values of 1.21, 1.21, 1.20, 1.18, and 1.15, respectively. This indicates that using T and O-I stiffeners increases the loads greatly. This could be because T-shaped stiffeners whether welded to outer or inner tubes increased the confinement due to the constraining effects of both O-I and T-shaped stiffeners. Therefore, the increase in the ultimate strength (N_u) is dependent on the type and arrangements of stiffening methods. In general, the use of longitudinal stiffeners could improve the strength and ductility of OCFDST stub columns. This could be mainly attributed to the improvement of the stiffness, restriction of the elastic-plastic buckling at lower loads as well as the confinement of the steel tube to the sandwiched concrete. It is concluded that the stiffeners can significantly contribute to the enhancement of strength along with achieving a reduction in the steel ratio (δ_s) resulting in lower cost, light construction, and higher performance of OCFDST short columns.

Comparison with the Existing Code Formulas

Eurocode 4

The design formula for circular CFST provided in EC4 [20] is adopted to predict the design ultimate strength of the studied OCFDST stub columns. The EC4 design formula is expressed in Eq. (17):

$$N_{uEC4} = \eta_{so} A_{so} f_{yo} + A_c f_c \left(1 + \eta_c \frac{t_o}{D_o} \frac{f_{yo}}{f_c} \right) + A_{si} f_{yi} \quad (17)$$

It is worth noting that the confinement of the inner steel tube to the strength of OCFDST stub columns is not considered in Eq. (17). It is only considered as an independent term in the design equation. The slenderness dependents η_{so} and η_c are determined by Eq. (18) and Eq. (19), respectively:

$$\eta_{so} = 0.25(3 + 2\lambda), \text{ but } \eta_{so} \leq 1 \quad (18)$$

$$\eta_c = 4.9 - 18.5\lambda + 17\lambda^2 \text{ but, } \eta_c \geq 0 \quad (19)$$

Where, $\bar{\lambda}$ denotes the relative slenderness limit, as defined in EC4 [20]. The effective length factor is taken as unity herein in order to reflect the FE simulation and experimental boundary conditions. The design formula in Eq. (7) is applicable for columns with a slenderness limit of $D_o/t_o \leq 90(235/f_{yo})(E_{so}/210000)$. In case the slenderness ratio exceeds this slenderness limit, an effective area (A_e) can be used for the outer steel tube, expressed by [36].

$$A_e = A_{so} \left(\frac{90}{t_o} \frac{235}{f_{yo}} \frac{E_{so}}{210000} \right)^{0.5} \quad (20)$$

Based on the basic superposition, the enhancement factor to the sandwiched concrete η_c in Eq. (17) was modified by [16] considering the equivalent circular section of the OCFST axial member. Hence, the modified formula in [16] is also adopted for OCFDST stub columns, expressed as:

$$N_{u,MECA} = \eta_{so} A_{so} f_{yo} + A_c f_c \left(1 + 0.73 \eta_c \frac{t_o}{D_o} \frac{f_{yo}}{f_c} \right) + A_{si} f_{yi} \quad (21)$$

American Specifications AISC360

The AISC360 [21] design code for concrete-filled steel composite members provided a design rule to calculate the ultimate capacity of CCFST columns under axial compression. The studied OCFDST stub columns are classified as compact, non-compact, and slender sections according to the limiting (D_o/t_o) values, as summarized in Table 5.

In this investigation, the AISC 360 design formula is adopted for the studied specimens with compact, non-compact and slender sections. The compact section has a slenderness limit of $D_o/t_o \leq \lambda_p$, which can approach the yield strength of steel tubes and exhibit a concrete compressive strength of $0.95 f_c$ due to higher confinement effect induced by the outer steel tube. The non-compact section has a slenderness limit of $\lambda_p < D_o/t_o \leq \lambda_r$, which can also attain the yield strength of steel tube and develop a concrete compressive strength between $0.95 f_c$ and $0.7 f_c$ due to less confinement than that of compact section due to local buckling [7, 37]. A slender section has a slenderness limit of $\lambda_r < D_o/t_o \leq \lambda_{max}$ and can neither reach the yield strength nor confine the concrete beyond $0.7 f_c$ [7, 38]. The design formula provided by AISC360 [21] is expressed as

$$N_{AISC} = \begin{cases} A_{so} f_{yo} + 0.95 A_c f_c + A_{si} f_{yi} & (Compact) \\ N_y + \frac{N_p - N_y}{(\lambda_r - \lambda_p)^2} (\lambda_r - \lambda)^2 + A_{si} f_{yi} & (Noncompact) \\ A_{so} f_{cr} + 0.7 A_c f_c + A_{si} f_{yi} & (Slender) \end{cases} \quad (22)$$

where, $\lambda = D_o/t_o$ is the slenderness of the equivalent circular section of the outer octagon steel tube. f_{cr} is the elastic critical buckling stress of outer octagonal steel tube, determined from Eq. (23), while N_p and N_y are calculated by Eq. (24) and Eq. (25), respectively.

Table 5. Limiting (D_o/t_o) in composite members under axial compression [7, 21]

Code	Compact/Non-compact (λ_p)	Non-compact/slender (λ_r)	Maximum (λ_{max})
AISC360	$\frac{0.15 E_{so}}{f_{yo}}$	$\frac{0.19 E_{so}}{f_{yo}}$	$\frac{0.31 E_{so}}{f_{yo}}$

Table 6. Limiting (w_o/t_o) in composite members under axial compression [35]

Code	Compact	Non-compact	Slender
ASCE/SEI 48	$\frac{w_o}{t_o} \leq \frac{681.2}{\sqrt{f_{yo}}}$ $f_{cr} = f_{yo}$	$\frac{681.2}{\sqrt{f_{yo}}} < \frac{w_o}{t_o} \leq \frac{919.62}{\sqrt{f_{yo}}}$ $f_{cr} = 1.42f_{yo} \left(1 - 0.000435 \sqrt{f_{yo}} \frac{w_o}{t_o} \right)$	$\frac{w_o}{t_o} > \frac{919.6}{\sqrt{f_{yo}}}$ $f_{cr} = \frac{724362}{\left(\frac{w_o}{t_o} \right)^2}$

where f_{cr} is the critical elastic stress.

$$f_{cr} = \frac{0.72 f_{yo}}{\left[\left(\frac{D_o}{t_o} \right) \frac{f_{yo}}{E_{so}} \right]^{0.2}} \quad (23)$$

$$N_p = A_{so} f_{yo} + 0.95 A_c f_c + A_{si} f_{yi} \quad (24)$$

$$N_y = A_{so} f_{yo} + 0.7 A_c f_c + A_{si} f_{yi} \quad (25)$$

Proposed Modification on the AISC360 Specifications

The compressive cross-sectional resistance provided by AISC360 can be modified herein for OCFDST stub columns considering the limit of w_o/t_o provided in ASCE 48-11 [35] for the octagonal section, as shown in Table 6.

DBJ/T13-51-2010

The design formula given by DBJ/T13-51-2010 [22] for circular CFST columns is also used to determine the axial capacities of the studied specimens, which are expressed by:

$$N_{u,DBJ} = (1 + 1.02 \xi_n) A_i f_c + A_{si} f_{yi} \quad (26)$$

Comparison of FE Results with the Predicted from Design Codes

According to the authors' best knowledge, there are no existing compressive design strength formulas for calculating the ultimate design strength of OCFDST stub columns. The FE results of such axial members are compared with the design strength predictions determined using the provisions of Eurocode 4 [20], modified EC4 [16], AISC360-16 [21], modified AISC360 and DBJ/T13-51-2010 [22], as summarized in Table 7. The comparison is also graphically illustrated in Figure 15, where the ratio of the calculated ultimate loads-to-the FE predicted ultimate strengths ($N_{u,code} / N_{u,FEM}$) has been plotted against the FE-predicted ultimate strengths ($N_{u,FEM}$). It can be seen that both EC4 [20] and modified EC4 [16] formula can accurately estimate the ultimate strength of OCFDST stub columns with wide variation of parameters with better prediction provided by the original EC4 formula. However, these provisions slightly provide conservative predictions of ultimate strength for specimens with different stiffening schemes. Similarly, the code, AISC360 and modified AISC360 significantly also give safe predictions for non-stiffened specimens and greatly underestimates the ultimate loads of stiffened specimens, while

Table 7. Overall comparison of the FE results with predictions from design codes

Column Label	FEM		EC4 [20]		Modified EC4 [16]		AISC360 [21]		Modified AISC360		DBJ [22]	
	$N_{u,FEM}$ (kN)	$N_{u,EC4}$ (kN)	$N_{u,EC4}$ $/N_{u,FEM}$	$N_{u,MEC4}$ (kN)	$N_{u,MEC4}$ $/N_{u,FEM}$	$N_{u,AISC}$ (kN)	$N_{u,AISC}$ $/N_{u,FEM}$	$N_{u,MAISC}$ (kN)	$N_{u,MAISC}$ $/N_{u,FEM}$	$N_{u,DBJ}$ (kN)	$N_{u,DBJ}$ $/N_{u,FEM}$	
OS00-to2	2845.28	2647.30	0.93	2594.74	0.91	2350.70	0.83	1890.89	0.66	3067.37	1.08	
OS00-to3	3155.35	3056.10	0.97	2978.50	0.94	2847.70	0.90	3019.19	0.96	3430.80	1.09	
OS00-to4	3513.88	3524.13	1.00	3422.30	0.97	3787.42	1.08	3738.16	1.06	3894.59	1.11	
OS00-to5	3901.24	4042.73	1.04	3917.48	1.00	4164.07	1.07	4164.07	1.07	4368.02	1.12	
OS00-ti2	2744.19	2785.70	1.02	2714.79	0.99	2557.41	0.93	2294.50	0.84	3154.77	1.15	
OS00-ti3	2903.67	2862.91	0.99	2792.00	0.96	2633.96	0.91	2371.05	0.82	3231.32	1.11	
OS00-ti4	3066.67	2939.42	0.96	2868.51	0.94	2709.82	0.88	2446.92	0.80	3307.19	1.08	
OS00-ti5	3225.46	3015.23	0.93	2944.32	0.91	2785.00	0.86	2522.09	0.78	3382.37	1.05	
OS00	2691.66	2960.75	1.10	2878.10	1.07	2600.66	0.97	2337.75	0.87	3475.39	1.29	
OS00-Di100	3024.88	3014.05	1.00	2937.18	0.97	2717.15	0.90	2454.25	0.81	3455.30	1.14	
OS00-Di100	3051.15	2977.43	0.98	2903.81	0.95	2717.12	0.89	2454.21	0.80	3378.42	1.11	
OS00-Di120	3068.56	2920.00	0.95	2850.36	0.93	2704.86	0.88	2441.96	0.80	3272.27	1.07	
OS00-Di140	3058.28	2841.69	0.93	2776.75	0.91	2680.40	0.88	2417.49	0.79	3136.82	1.03	
OS00-Di160	3033.15	2742.55	0.90	2683.02	0.88	2643.72	0.87	2380.81	0.78	2972.08	0.98	
OS00-Di180	2985.6	2622.74	0.88	2569.36	0.86	2594.82	0.87	2331.92	0.78	2861.73	0.96	
OS00-Di200	2907.42	2482.52	0.85	2436.00	0.84	2533.71	0.87	2270.81	0.78	2628.25	0.90	
OP1S00	4026.18	3517.72	0.87	3440.13	0.85	3309.33	0.82	3480.82	0.86	4006.57	1.00	
OP1S30	4258.65	3554.46	0.83	3483.55	0.82	3324.86	0.78	3061.96	0.72	4031.86	0.95	
OP2S57	4259.11	3692.54	0.87	3621.62	0.85	3462.94	0.81	3200.03	0.75	4060.30	0.95	
OP3TO4	4296.76	3521.13	0.82	3450.21	0.80	3291.53	0.77	3028.62	0.70	3888.89	0.91	
OP3TI4	4200.4	3521.13	0.84	3450.21	0.82	3291.53	0.78	3028.62	0.72	3888.89	0.93	
OTO8	4132.18	3516.37	0.85	3445.46	0.83	3286.77	0.80	3023.86	0.73	3884.13	0.94	
Mean			0.93		0.91		0.88		0.81		1.04	
Standard Deviation (SD)			0.073		0.069		0.079		0.100		0.096	

it slightly underestimates the capacities of specimens with different types and arrangements of stiffeners. DBJ formula yields more un-conservative predictions of ultimate strengths for the unstiffened specimens with varying outer tube thickness, thickness, and diameter of the inner tube. DBJ equation greatly overestimates the ultimate strength of OS00 (CFST stub column). However, DBJ provisions give accurate results of the OCFDST stub columns with different stiffening schemes. As given in Table 7, it can be seen that the mean ratios ($N_{u,code} / N_{u,FEM}$) for EC4, modified EC4, modified AISC360, and DBJ formula are 0.93, 0.91, 0.88, 0.81, and 1.04 with corresponding standard deviation (SD) values of 0.073, 0.069, 0.079, 0.1, and 0.096, respectively. This confirms that EC4 and modified EC4 formulas can safely be used to predict the design ultimate strength of OCFDST stub columns. AISC360 can also give a reasonable for non-stiffened specimens while, DBJ provides un-conservative predictions of ultimate strength when applied to non-stiffened OCFDST stub columns, while it can accurately predict the ultimate strength of the OCFDST axial members with different stiffening schemes. Overall, it can be confirmed that all design codes except DBJ can safely predict the strength of un-stiffened specimens and underestimate the strength of specimens with different stiffening schemes. This could be because the contribution

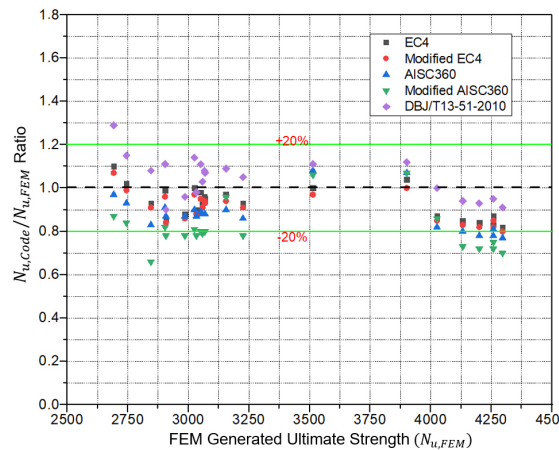


Figure 15. Overall comparison between the FE results with strength predictions from design codes.

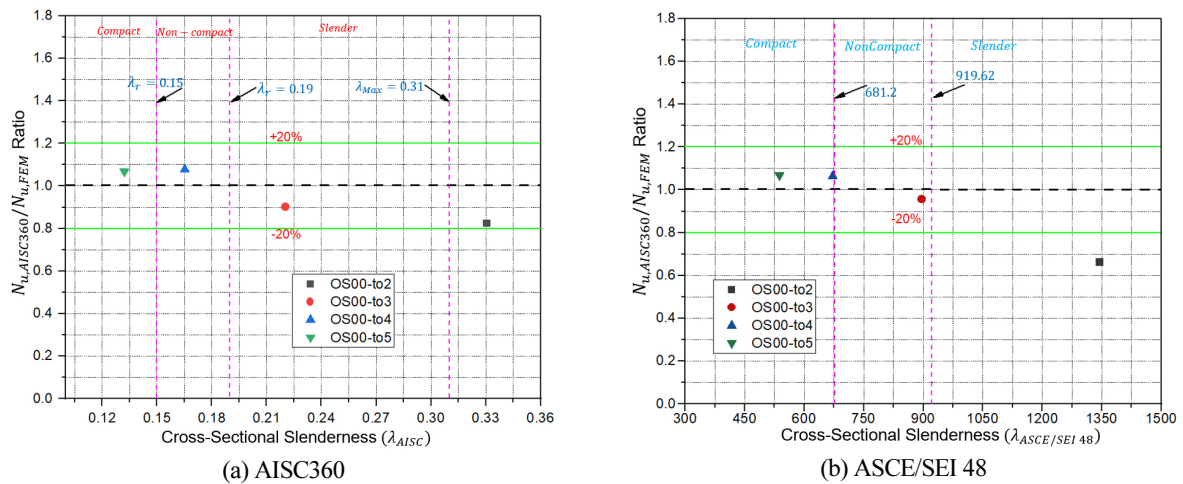


Figure 16. Comparison of FE results with strength predictions from design codes with different values of cross-sectional slenderness.

of stiffeners was considered as an additional term of $(A_{ss} f_{yso})$ in the calculation of the ultimate strength. Hence, the contribution of welded stiffeners and arrangement to the confinement of steel tubes were not considered by the design codes.

The accuracy of AISC360 and modified AISC360 is further assessed by comparing the FE results with their design strength formula provisions considering the provided cross sectional slenderness range, as shown in Figure 16, in which the ratios of FE results to the strength predictions from design formulas are plotted against the cross-sectional slenderness $\lambda_{AISC360} = (D_o/t_o)(f_{y_o}/E_{s_o})$ and $\lambda_{ASCE/SEI48} = (w_o/t_o)(\sqrt{f_{y_o}})$ provided by AISC360 and ASCE 48-11 [35], respectively. It can be seen from Figure 16 that both AISC360 and modified AISC360 provide safe predictions of ultimate strengths of OCFDST stub columns with compact and non-compact sections. AISC360 yields very conservative predictions of ultimate strength of the slender section, while modified AISC360 significantly underestimates the strength of slender section.

Conclusion

The current paper provides an extensive evaluation of OCFDST stub columns to address their behavior under axial compression and the following conclusions can be drawn:

- a) The numerically generated axial load-deformation ($N-\Delta$) curves show a well agreement with those obtained from tests. Ultimate loads $N_{u,FEM}$ obtained from numerical simulations are closed with those of experiment $N_{u,exp}$ with a mean ratio of ($N_{u,FEM}/N_{u,exp}$) of 0.97 and corresponding standard deviation (SD) of 0.004. Therefore, a subsequent parametric study was conducted in order to investigate the effects of different parameters including the thickness of the outer steel tube (t_o), thickness of inner steel tube (t_i), the diameter of inner steel tube (D_i) and type and arrangement of stiffening schemes.
- b) It was found that using thicker out steel tubes can impose a higher confinement effect on the sandwiched concrete resulting in higher ultimate strength (N_u) and ductility.
- c) It was also noticed that enlarging the thickness of the inner steel tube (t_i) can result in a considerable enhancement on the ultimate strength (N_u) of OCFDST stub columns with a minor ductility improvement. This could be because using thicker inner tube does not contribute to the confinement of sandwiched concrete and only affects the strength of OCFDST stub columns rather than their ductility.
- d) In addition, it can be observed that the strengths of OCFDST stub columns significantly increase with increasing the diameter of inner tube (D_i) up to 140 mm. However, further increase in D_i can adversely affect the strength of OCFDST short axial members.
- e) Besides, it was observed that the stiffeners can significantly contribute to the enhancement of strength with achieving a reduction in the steel ratio (δ_s) resulting in the achievement of lower cost, light construction, and higher performance of OCFDST short columns.
- f) Both EC4 and modified EC4 formulas yield the most accurate predictions of ultimate loads for non-stiffened specimen, while, AISC360 and modified can also give a reasonable for non-stiffened specimens. However, DBJ provides un-conservative predictions when applied to OCFDST stub columns. It was also observed that all design codes except DBJ, underestimate the capacities of stiffened specimens with slender sections.

It can be concluded that the developed FE model in this study provides the benchmark numerical results for the design of OCFDST stub columns. Further experimental program on OCFDST columns with high and ultra-high-strength concretes and high-strength steel is required.

Acknowledgments

The authors would like to gratefully acknowledge the support of this research provided by graduate scientific research and innovation foundation of Chongqing, China (Grant No. CYB19016) and the funding support from the Chongqing Talents Plan for Young Talents (No. CQYC201905055).

References

- [1] M.F. Hassanein, O.F. Kharoob, and Q.Q. Liang, *Circular concrete-filled double skin tubular short columns with external stainless-steel tubes under axial compression*. *Thin-Walled Structures*. 73(2) (2013), pp. 52-263. DOI: 10.1016/j.tws.2013.08.017.
- [2] X.-L. Zhao and L.-H. Han, *Double skin composite construction*. *Progress in Structural Engineering and Materials*. 8(3) (2006), pp. 93-102. DOI: 10.1002/pse.216.
- [3] F. Wang, L. Han, and W. Li, *Analytical behavior of CFDST stub columns with external stainless-steel tubes under axial compression*. *Thin-Walled Structures*. 127 (2018), pp. 756-768. DOI: 10.1016/j.tws.2018.02.021.
- [4] Z. Tao, B. Uy, L.-H. Han, and Z.-B. Wang, *Analysis and design of concrete-filled stiffened thin-walled steel tubular columns under axial compression*. *Thin-Walled Structures*. 47(12) (2009), pp. 1544-1556. DOI: 10.1016/j.tws.2009.05.006.
- [5] F. Yuan, H. Huang, and M. Chen, *Behavior of square concrete-filled stiffened steel tubular stub columns under axial compression*. *Advances in Structural Engineering*. (2019), 136943321881958. DOI: 10.1177/1369433218819584.
- [6] S. Alqawzai, K. Chen, L. Shen, M. Ding, B. Yang, and M. Elchalakani, *Behavior of octagonal concrete-filled double-skin steel tube stub columns under axial compression*. *Journal of Constructional Steel Research*. 170 (2020), pp. 106-115. DOI: 10.1016/j.jcsr.2020.106115.
- [7] F. Wang, B. Young, and L. Gardner, *Compressive testing and numerical modelling of concrete-filled double skin CHS with austenitic stainless-steel outer tubes*. *Thin-walled Structures*. 141 (2019), pp. 345-359. <https://doi.org/10.1016/j.tws.2019.04.003>.
- [8] M. Elchalakani, V. Patel, A. Karrech, M. Hassanein, S. Fawzia, and B. Yang, *Finite Element Simulation of Circular Short CFDST Columns under Axial Compression*, Elsevier, *Structures*. (2019), pp. 607-619.
- [9] Q.Q. Liang, *Nonlinear analysis of circular double-skin concrete-filled steel tubular columns under axial compression*. *Engineering Structures*. 131 (2017), pp. 639-650. DOI: 10.1016/j.engstruct.2016.10.019.
- [10] M. Ahmed, Q.Q. Liang, V.I. Patel, and M.N.S. Hadi, *Numerical analysis of axially loaded circular high strength concrete-filled double steel tubular short columns*. *Thin-Walled Struct.* 138 (2019), pp. 105-116.
- [11] M. Elchalakani, M.F. Hassanein, A. Karrech, S. Fawzia, B. Yang, and V.I. Patel, *Experimental tests and design of rubberised concrete-filled double skin circular tubular short columns*. *Structures*. 15 (2018), pp. 196-210. DOI: 10.1016/j.istruc.2018.07.004.
- [12] M. Elchalakani, X.L. Zhao, and R.H. Grzebieta, *Tests on Concrete-filled Double-Skin Composite Short Columns under Axial Compression*. *Thin-Walled Structures*. 40(5) (2002), pp. 415-441.
- [13] M. Elchalakani, M.F. Hassanein, A. Karrech, and B. Yang, *Experimental investigation of rubberised concrete-filled double skin square tubular columns under axial compression*. *Engineering Structures*. 171 (2018), pp. 730-746. DOI: 10.1016/j.engstruct.2018.05.123.
- [14] F. Wang, B. Young, and L. Gardner, *Experimental study of square and rectangular CFDST sections with stainless steel outer tubes under axial compression*. *Journal of Structural Engineering, ASCE*. 145(11) (2019), 04019139. [http://dx.doi.org/10.1061/\(ASCE\)ST.1943-541X.0002408](http://dx.doi.org/10.1061/(ASCE)ST.1943-541X.0002408).
- [15] F. Ding, Z. Li, S. Cheng, and Z. Yu, *Composite action of octagonal concrete-filled steel tubular stub columns under axial loading*. *Thin-Walled Structures*. 107 (2016), pp. 453-461. DOI: 10.1016/j.tws.2016.07.012.
- [16] J.-Y. Zhu and T.-M. Chan, *Experimental investigation on octagonal concrete filled steel stub columns under uniaxial compression*. *Journal of Constructional Steel Research*. 147 (2018), pp. 457-467. DOI: 10.1016/j.jcsr.2018.04.030.
- [17] M.F. Hassanein, V.I. Patel, M. Elchalakani, and H.-T. Thai, *Finite element analysis of large diameter high strength octagonal CFST short columns*. *Thin-Walled Structures*. 123 (2018), pp. 467-482. DOI: 10.1016/j.tws.2017.11.007.

- [18] J. Yang, H. Xu, and G. Peng, *Behavior of concrete-filled double skin steel tubular columns with octagon section under axial compression*. *Frontiers of Architecture and Civil Engineering in China*. 2(3) (2008), pp. 205-210. DOI: 10.1007/s11709-008-0035-5.
- [19] W. Yuan and J. Yang, *Experimental and numerical studies of short concrete-filled double skin composite tube columns under axially compressive loads*. *Journal of Constructional Steel Research*. 80 (2013), pp. 23-31. DOI: 10.1016/j.jcsr.2012.09.014.
- [20] EN1994-1-1, *Eurocode4 Design of Steel and Concrete Structures, Part1.1*, General rules and rules for buildings, European Committee for Standardization CEN, Brussels, 2004.
- [21] ANSI/AISC 360-16, *Specification for Structural Steel Buildings*, American Institute of Steel Construction, Chicago, USA, 2016.
- [22] DBJ/T 13-51-2010, *Technical Specification for Concrete-filled Steel Tubular Structures*, The Department of Housing and Urban-Rural Development of Fujian Province, Fuzhou (China) (in Chinese), 2010.
- [23] V.I. Patel, B. Uy, K.A. Prajwal, and F. Aslani, *Confined concrete model of circular, elliptical and octagonal CFST short columns*. *Steel and Composite Structures*. 22(3) (2016), pp. 497-520.
- [24] J.B. Mander, M.N.J. Priestly, and R. Park, *Theoretical stress-strain model for confined concrete*. *Journal of Structural Engineering, ASCE*. 114(8) (1988), pp. 1804-1826.
- [25] J.C. Lim and T. Ozbakkaloglu, *Stress-strain model for normal-and light-weight comunder uniaxial and triaxial compression*. *Construction Building Materials*. 71 (2014), pp. 492-509.
- [26] M. Ahmed, Q.Q. Liang, V.I. Patel, and M.N.S. Hadi, *Nonlinear analysis of rectangular concrete-filled double steel tubular short columns incorporating local buckling*. *Journal of Structural Engineering*, 175 (2018), pp. 13-26.
- [27] Q.Q. Liang, *Performance-based analysis of concrete-filled steel tubular beam-columns, Part I: Theory and algorithms*. *Journal of Constructional Steel Research*. 65(2) (2009), pp. 363-372.
- [28] Q.Q. Liang and S. Fragomeni, *Nonlinear analysis of circular concrete-filled steel tubular short columns under axial loading*. *Journal of Constructional Steel Research*. 65(12) (2009), pp. 2186-2196.
- [29] F.E. Richart, A. Bradtzaeg, and R.L. Brown, *A study of the failure of concrete under combined compressive stresses*. Bull. 185 (1928). Champaign (III): University of Illionis, Engineering Experimental Station.
- [30] H.T. Hu, C.S. Huang, M. Wu, and Y. Wu, *Nonlinear analysis of axially loaded concrete-filled tube columns with confinement effect*. *Journal of Structural Engineering, ASCE*. 129(10) (2003), pp. 1322-1329.
- [31] X. Dai and D. Lam, *Numerical modelling of the axial compressive behaviour of short concrete-filled elliptical steel columns*. *Journal of Constructional Steel Research*. 66(7) (2010), pp. 931-942.
- [32] Z. Tao, Z.B. Wang, and Q. Yu, *Finite element modelling of concrete-filled steel stub columns under axial compression*. *Journal of Constructional Steel Research*. 89 (2013), pp. 121-131.
- [33] Y.-B. Zhang, L.-H. Han, K. Zhou, and S. Yang, *Mechanical performance of hexagonal multi-cell concrete-filled steel tubular (CFST) stub columns under axial compression*. *Thin-Walled Structures*. 134 (2019), pp. 71-83. DOI: 10.1016/j.tws.2018.09.027.
- [34] D.H. Nguyen, W.-K. Hong, H.-J. Ko, and S.-K. Kim, *Finite element model for the interface between steel and concrete of CFST (concrete-filled steel tube)*. *Engineering Structures*. 185 (2019), pp. 141-158.
- [35] ASCE/SEI, *Design of steel transmission pole structures*. ASCE/SEI 48. Reston, VA: ASCE/SEI, 2011.
- [36] BS 5950-1, *Structural Use of Steelwork in Building-Part 1: Code of Practice for Design-Rolled and Welded Sections*, The Standards Policy and Strategy Committee, 2000.
- [37] W.F. Chen and D.J. Han, *Plasticity for Structural Engineers*. J. Ross Publishing. NewYork, USA, 2007.
- [38] Z. Lai, A.H. Varma, and K. Zhang, *Noncompact and slender rectangular CFT members: Experimental database, analysis, and design*. *Journal of Constructional Steel Research*. 101 (2014), pp. 455-468. DOI: 10.1016/j.jcsr.2014.06.004.